Field and central receiver design methodology based on multi-parameter optimization by the design of experiments (DOE) technique

Rubén Barbero[a], Guillermo Ortega[b], Fernando Varela[c], Antonio Rovira[d]

[a] Universidad Nacional de Educación a Distancia (UNED), Madrid, Spain, rbarbero@ind.uned.es. (CA)
[b] Universidad de Huelva (UHU) Huelva, Spain. guillermo@didp.uhu.es
[c] Universidad Nacional de Educación a Distancia (UNED), c/ Juan del Rosal, 12, 28040 Madrid, Spain, fvarela@ind.uned.es
[d] Universidad Nacional de Educación a Distancia (UNED), c/ Juan del Rosal, 12, 28040 Madrid, Spain, rovira@ind.uned.es

Abstract:

This manuscript presents a novel methodology for the design of Central Tower Receivers (CTR), which involves simplified models for optical and thermal calculations and evaluation of design constraints. The proposed methodology optimizes the total yearly energy production as the criterion, considering a multi-parameter analysis. This design is part of the AdInCCSol (Advanced Integration of Combined Cycles in Solar thermal power plants) project, which aims to integrate advanced thermodynamic cycles in solar thermal power plants to improve efficiencies and lower LCOE. Specifically, the manuscript presents the optimization of a 100 MW CTR plant based on a conventional cylindrical receiver that operates at an outlet temperature of 565 ºC. Unlike previous studies, the proposed methodology considers yearly calculations and takes into account most of the parameters that affect thermal and optical efficiencies, including tube diameter, receiver diameter, height, and the number of faces. The aiming strategy for each design was also optimized to achieve the best balance between optical and thermal losses while meeting stress and corrosion limits. The study was conducted using two in-house codes that integrate thermal and optic performance calculations and models for estimating design constraints, providing accurate results with low running times. The findings of the study indicate the presence of an optimal receiver area that optimizes the design for a target power of concentrated radiation flux density. Moreover, certain combinations of parameters yield similar yearly energy productions, enabling the development of designs with comparable performance and reduced costs.

Keywords:

Central Tower Receiver (CTR), aiming strategy, receiver design optimization, heliostat field

1. Introduction

This paper presents a study focused on designing an optimized central tower receiver for the AdInCCSol project. The objective is to analyze multiple parameters and optimize the receiver design in terms of yearly performance.

Designing a solar thermal power plant is a complex task that requires the integration of multiple models and tools from various multidisciplinary fields since the optimal solution depends on several parameters. One of the key challenges is that the optical and thermal performance cannot be optimized independently. Also, structural stresses or corrosion inside the tubes can cause receiver failure [1-3], while pressure drop and flow stability inside the tubes can lead to operational issues [2,4]. Therefore, it is essential to integrate all these calculations into the design process to achieve the desired performance.

The heliostat field design and aiming strategy are crucial for an optimal design. Firstly, it is important to establish the Allowable Density Flux (AFD) [5-6], to adapt the flux maps to this limit, maximizing thermal

https://doi.org/10.52202/069564-0149

performance and minimizing ray spillages. The strategy of adapting the aiming points of the heliostats can vary from different authors from more simple approximations [7] to more complex ones like the one based on Deviation-based Aiming Strategy (DBA) [8-9]. Again, the optimization of the aiming strategy involves the integrated analysis of the optical and thermal performances.

Over the last four decades, some algorithms have been developed oriented toward the optimization of the heliostat field [10]. However, up to the authors' knowledge, there are no studies that proposed a receiver design based on an optimization process coupling heliostat field and aiming strategy optimization with thermal performance analysis and considering stress and corrosion limits.

The present study describes the design of a solar thermal power plant with a standard configuration of 100 MWe in Seville. To achieve this, the power output is divided into two towers and their respective fields to avoid very large distances from the heliostats to the receiver that would be subjected to an important attenuation. In addition, the flexibility that adds a dual-tower system [11] is another aspect that can be considered in this project. Specifically, each tower is designed to produce 340 MW of concentrated radiation and 300 MWt of thermal output for the fluid, resulting in a Solar Multiple (SM) of 1.2. Doubling the tower produces an optimal SM of 2.4, which is suitable for 8 hours of storage [12].

Two already developed tools were adapted to this methodology and are described in section 2, while the methodology for the design is established in section 3. The results are introduced an analyzed in section 4 to obtain an optimum combination of design parameters and orientate the final design of the receiver.

This work represents a significant contribution to the field of Central Tower Systems (CTS) design for Concentrated Solar Power (CSP) by presenting an efficient methodology for designing CTRs and considering multiple parameters in the optimization. One of the novelties is the use of a Design of Experiments (DOE) methodology for the optimization, which contributes to having more information about the effect of the different parameters over the global performances.

2. Heliostat field and receiver modeling

In this project, two different tools have been used to facilitate the design process. One of the tools was specifically adapted for the optical optimization of the field and receiver aiming strategy. The other tool was dedicated to the thermal performance of the receiver and included integrated calculations to predict structural limits, flow stability issues, and pressure drops. By utilizing these tools in combination, a more comprehensive understanding of the solar thermal power plant design was achieved, allowing for an optimized solution that meets the requirements.

The subsequent sub-sections outline the models and tools utilized in the study, while the methodology section describes their integration and iterative process to obtain an optimal solution.

2.1. Optical modeling and optimization of the heliostat field. Aiming strategy.

Two software applications developed in Matlab 2022b have been employed.

- An application for optimizing the layout of heliostats.
- An application for optimizing the aiming strategy.

The first one, HRT (Homology Ray-Tracing) code is used for the optics optimization and is based on the yearly insolation weighted efficiency as a Function Of Merit (FOM), which according to [13] and [14], is given by Eq. (1):

$$\eta_{yearly\_w} = \frac{\sum_{d=1}^{365} \int_{orto}^{ocaso} \eta(t) \cdot IND(t)}{\sum_{d=1}^{365} \int_{orto}^{ocaso} IND(t)}, \quad (1)$$

where η (t) is the instantaneous optical efficiency and IND (t) represents the instantaneous beam insolation, Eq. (2).

$$\eta_{(t)} = \frac{\sum_{1}^{N} (\eta_{cos} \cdot \eta_{ref} \cdot \eta_{s\&b} \cdot \eta_{aa} \cdot \eta_{int})}{N}. \quad (2)$$

In general, the optimization code operates by proposing an array or pattern of heliostats in the field, according to parameterized expressions. These allow the location of each of the heliostats in the array to be determined within geometric limits on the horizontal plane, which are usually a function of the tower height and the geometry of the receiver [15, 16]. Typically, the proposed field layout comprises a greater number of heliostats than those required to reach the target power at the design point [13, 14, 17].

Next, the subset of heliostats of the proposed field is determined that, with greater optical efficiency, allows obtaining the target power on the receiver at the design point (autumn equinox at solar noon). Subsequently, operating with this subset of heliostats, the merit function is evaluated using multiple sample points. Since the initial field is as compact as possible, the overall efficiency can be improved, as significant losses due to

shading and blockages will occur, while the remaining elementary efficiencies (cosine factor, reflection, atmospheric attenuation, and interception) are very high. Then, the optimization code proposes another configuration or pattern, differing slightly from the previous one, and the calculations are repeated.

To reduce computation time, the code implements various resources, such as techniques to reduce the number of candidates in determining to shade and blocking performances [18], homographic techniques for determining interception and shading and blocking performance [19] and [20], or evaluating the merit function using numerical integration methods [21].

Starting from an optimized layout, the aiming strategy is optimized using the aforementioned second application. For this purpose, an iterative process is used, which consists of the following steps:

1. Several sample points are used to simulate in detail each of the heliostats in the solar field aiming at the receiver center and determine the power density matrices of each heliostat.
2. Correct the aiming in the vertical direction.
3. Recalculate the power density matrices and efficiencies of each heliostat.

In this case, a detailed Monte-Carlo Ray Tracing (MCRT) is used, with few simplifications. 10,000 rays per heliostat have been used. Other features of this ray-tracing include:

- Uses the MCRT methodology.
- Assumes that the surface of the heliostat has a rectangular shape and elliptical quadric curvature without holes or discontinuities (a spherical surface is considered in this case with on-axis cant).
- Incident rays are randomly generated following a Standard Solar Model (SSM). A Gaussian SSM with σ = 2.325 mrad has been considered.
- The incident rays are randomly generated uniformly over the surface of the heliostat.
- The optical errors (macroscopic and microscopic) associated with the reflecting surface of the heliostat are considered by using Gaussian distributions in both cases. Values of σ = 2.0 and 1.0 mrad for the macroscopic and microscopic, respectively, are used.
- The reflectivity of the heliostat, as well as the losses due to atmospheric attenuation, are applied in a non-deterministic manner.
- Both the methodology used for preselecting candidates for shading and blocking, as well as the methodology used for determining to shade and blocking, are defined in [19].

This sub-process dedicated to correcting the aiming in the vertical direction consists of the following steps: a ϕ_{obj} matrix of size m·n is defined, whose cells have the value given by Eq. (3).

$$\phi_{obj} = coef \cdot \frac{Total\ power\ over\ the\ receiver}{receiver\ area}. \tag{3}$$

Where *coef* is a user-defined value. The φ matrix of size m·n is initialized with null values, where m represents half of the number of vertical cells and n is the number of heliostats. An iterative process is started that goes through the n heliostats of the solar field ordered from highest to lowest total optical efficiency. The vertical location of the power density matrix of the i-th heliostat ϕ_i that minimizes the Root Mean Square (RMS) value is determined, by minimizing Eq. (4).

$$RMS = \sqrt{\sum_1^m \left(\sum_1^n \varphi + \phi_i - \phi_{obj}\right)/(m \cdot n)}. \tag{4}$$

Once the RMS is minimized the aiming vertical position for each heliostat is updated, using Eq. (5).

$$\varphi = \varphi + \phi_i. \tag{5}$$

The aiming vertical correction for the i-th heliostat is determined trigonometrically and stored. This is repeated for different values of coef.

2.2. Thermal modeling of the receiver

The thermal performance for a region of uniform absorbed radiation can be obtained using Eq. (6) [22].

$$\eta(x^*) = \frac{\eta_0 \cdot g'(Z)}{(1-g'(Z))} \cdot \frac{1}{NTU \cdot x^*} \cdot \left(e^{\frac{1-g'(Z)}{g'(Z)} \cdot NTU \cdot x^*} - 1 \right), \tag{6}$$

The thermal efficiency at the inlet denoted as η_0, is a key performance parameter for a thermal system. In this context, the derivative of the characteristic function, g'(z), and z, the variable of this function, are defined in [22], while NTU (Number of Transfer Units) is a characteristic parameter of the thermal system and x^* is the non-dimensional coordinate.

To model the system, external heat transfer coefficients are required to evaluate the different terms of the characteristic function. However, it should be noted that the heat transfer mechanisms at the receiver are

https://doi.org/10.52202/069564-0149

complex due to the non-uniform absorption of radiation. Consequently, a dense mesh is needed to precisely evaluate the temperature at the tube surfaces. Furthermore, the receiver tubes are exposed to ambient air at the front and are insulated at the back with a panel that is separated from them. As a result, the air can enter through the gaps situated among the tubes and refrigerate them. The complexity of the convective currents around the receiver tubes, the coupling with radiation, the large dimensions of the receiver, and its open configuration are some of the reasons that support the idea that to accurately capture convection heat transfer it is required to perform unaffordable simulations by Computational Fluid Dynamics (CFD). The radiation mechanisms are also complex because different sections of the surface have varying view factors concerning the sky, the heliostats, the ground, the neighbor tubes, or the insulation at the back part. In this study, it was decided to introduce some simplifications as the purpose is not to achieve precise results, but rather approximations that allow comparison of different designs with rapid yearly calculations to optimize the design. To this end, the following hypotheses are considered for radiation and convection heat transfer:

- The tube is painted with Pyromark, with a constant emissivity of 0.87 in the range of temperatures of the receiver, and a solar absorptivity of 0.96 [23].
- The front face of the tube exchanges radiation with an equivalent surface at ambient temperature.
- The back face of the tube is considered insulated.
- Heat transfer by convection is assumed to be constant and equal to 14 W/(m^{2}K), as it is proposed in [24] for the DELSOL code.

The same set of hypotheses for the evaluation of thermal losses was considered and validated in [25], with the only difference of the values of the convective heat transfer coefficient that could vary.

Due to the non-uniform absorption of radiation in the receiver, the tube length is discretized into slices of 0.5 m where radiation flux density is averaged.

The fluid used is the "Solar salt", 60% $NaNO_3$ and 40% KNO_3, which thermo-physical properties are based on [1]. The fluid flow rate is adjusted to achieve the desired outlet temperature (565 ºC). However, under conditions of low absorbed radiation, the fluid flow may not be sufficient to adequately cool the receiver tube, leading to potential structural or corrosion limitations being exceeded. To prevent this, a threshold concentration of radiation at 160 MW (47% of the nominal value) has been established, below which the fluid flow rate is maintained at a constant value and the outlet temperature is allowed to vary accordingly.

The Direct Normal Irradiance (DNI) and temperature data for the location of Seville were obtained from the Typical Meteorological Year International Weather for Energy Calculation (TMY IWEC) database [26] and used as inputs in the simulations for all cases analyzed.

2.3. Design constraints

In concentrated solar power systems, receiver tubes are exposed to solar radiation and undergo thermal stresses that can lead to failure. The axial thermal stresses in the tubes can be eliminated with proper design. However, the temperature gradient in the tubes leads to maximum thermal stresses at the front or crown, estimated via a superposition of circumferential and radial gradients. Equation (7) has been adopted by multiple authors [4, 6-7].

$$\sigma_c = \gamma \cdot E \cdot \left[(\bar{T}_c - \bar{T}_w) + \frac{\Delta T_c}{2 \cdot (1-\nu)} \right]. \quad (7)$$

Where ν is the Poisson's ratio, γ is the coefficient of thermal expansion (mm/m·K) and σ_c is the thermal stress at the crown (MPa). The radial temperature difference at the crown (ΔT_c), the mean temperature at the crown (T_c), and the average tube temperature (T_w) are based on the local absorbed radiation and assuming that the backside temperature of the tube wall is the same as the working fluid temperature [4, 6-7]. These values are compared with Ultimate Tensile Strength (UTS) values for the tube material [27]. In this case Inconel 625 is selected for the tubes as it presents better performance to corrosion than, for example, Haynes 230, although this alternative presents better mechanical performance [7].

The corrosion of tubes is also a significant concern as it is accelerated by high temperatures. The material loss due to corrosion is limited to 0.5 mm over 10 years, and the temperature limit for corrosion of Inconel 625, used for the tubes, is 628 ºC [7]. These two limits are used to calculate the Allowable Flux Densities (AFD) for each node along the tube [7]. The radiation flux density at each node is compared to its allowable value, and the flux is reduced uniformly to meet this criterion. Although selective defocusing could be included in future studies.

Pressure loss is another critical factor, as a pressure of 20 bar is required to ensure correct solar field operation. Pressure losses are estimated for receiver tubes, headers, and elbows that appear in a standard, using the models proposed in [2].

Finally, downward flow inside the tubes may be subject to instabilities due to the upward buoyancy force, which tends to increase as flow velocity decreases. Perturbations in a downward-flow tube lead to the increased temperature inside the tube and buoyancy force, further decreasing the flow rate and potentially leading to

flow imbalance and operational problems in the receiver. The stability criterion proposed in [4] is included in the model to ensure that the downward flow inside the tubes is not subjected to instabilities. The criterion is expressed as follows, Eq. (8).

$$\frac{32 \cdot f}{\pi^2 \cdot d_i^5 \cdot \rho^2 \cdot g \cdot \beta} \cdot \dot{m}^2 / \Delta T \geq 1. \quad (8)$$

where f is the friction factor (-), di is the internal tube diameter (m), ρ is the fluid density in (kg/m3), $\dot{m}$ is the mass flow (kg/s), ΔT is the temperature difference (K), and L is the length of the tube (m).

3. Methodology

As was already introduced the proposed methodology was developed to optimize the heliostat field and receiver designs for a power plant located in Seville with a target thermal power of 300 MWt for each receiver, which implies a SM of 2.4. The design involves the analysis and optimization of three key parameters of the receiver, namely the receiver diameter (D), receiver height (H), and the number of faces (N). The optimization process is carried out in three steps. Firstly, the heliostat field is optimized for each of the receiver's diameters and heights using the code described in the previous section. Secondly, an appropriate aiming strategy is determined to maximize yearly energy production, and finally, a response surface is constructed and optimized using the results from all the simulations.

It is noteworthy that the effect of radiation flux densities changes from high to low temperatures, as shown in Fig. 1. The thermal performance for low temperatures due to a four-times reduction in radiation flux densities is found to be around 8%. In contrast, a two-times reduction for high temperatures leads to a significant reduction in performance, up to 20%. Thus, it is crucial to adopt a concentration level that optimizes thermal efficiency while avoiding optical losses for the operation over the whole year.

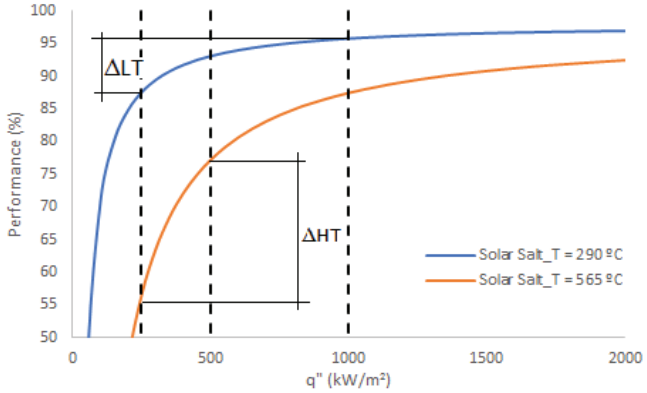

Figure 1. Thermal performance as a function of radiation flux density

To address the non-uniform distribution of the flux densities along the height of the receiver, a correction coefficient is proposed in this study, as described in section 2.1. This coefficient is designed in such a way that lower values indicate a tendency towards a uniform distribution (Figure 2 and Table 2). However, such uniformity can lead to an increase in optical losses due to ray spillage. On the other hand, higher values of the correction coefficient generate a narrower distribution with improved optical efficiency, but problems with the limits for tube failure. Thermal efficiency can increase or decrease depending on the shape of the distribution and receiver height. As a result, a search for the optimal value of this coefficient can be performed for a given set of parameters. Figure 2 shows the density flux maps for different values of the coefficient, while Table 2 summarizes the performance values of each of the maps.

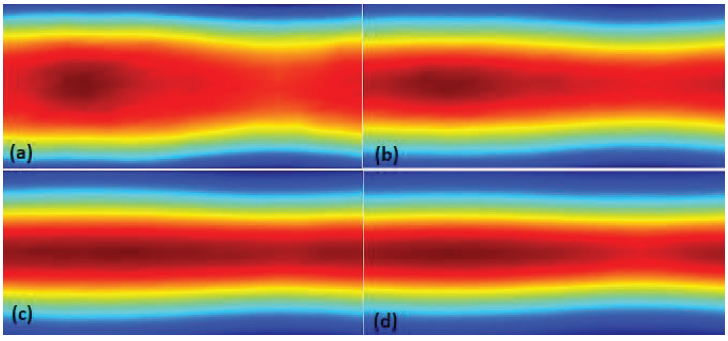

Figure 2. Density flux maps for different values of the coefficient

https://doi.org/10.52202/069564-0149

Table 2. Performance values for different coefficients in a general case

Coefficient	Thermal efficiency (%)	Optical efficiency (%)	Total efficiency (%)	Number of hours operation over the limit (h)
0.8	85.95	51.16	43.97	0
1.0	86.4	55.46	47.92	144
1.2	86.76	55.46	48.12	412
1.4	87.08	55.46	48.3	600

As it was said before, the operation over the tube failure limit is not permitted and radiation flux density is reduced for these instants, so the yearly energy produced would be diminished as this number increased, although optical and thermal efficiencies are greater. The operation under these conditions was limited to a maximum value of 10%, except in those cases with a small receiver, because the radiation flux density is very high. In any case, the influence of these cases on the optimization process is very limited, as It is shown in the next sections.

The optimization of the receiver design is carried out based on the yearly energy produced by the system, which is the main objective of this study. It is crucial to consider the system's performance under non-nominal conditions, as demonstrated in Fig. 1. The system's efficiency drops significantly when the absorbed radiation falls below a certain threshold, which is higher in the case of high temperatures.

The proposed methodology involves computationally expensive and time-consuming simulations. Therefore, the Design Of Experiments (DOE) methodology is preferred in this study due to its ability to reduce computational cost while providing a comprehensive understanding of the system's performance over a year. A face-centered central composite design algorithm is used to establish the case matrix which is composed of 15 cases (Table 3). The results of these cases are used to construct a second-grade polynomial function of three variables as a response surface for the yearly energy produced, which is then optimized.

Table 3. Case matrix from the face-centered central composite algorithm.

Cases	D (m)	H (m)	Number of faces	D tube (mm)	Gap (mm)	Number of tubes
1	8	10	10	36	0.9	670
2	15	10	10	22	1.06	2010
3	8	18	10	36	0.9	670
4	15	18	10	22	1.18	2000
5	8	10	18	57	2.4	414
6	15	10	18	34	1.2	1332
7	8	18	18	57	2.4	414
8	15	18	18	34	1.2	1332
9	8	14	14	46	0.85	532
10	15	14	14	28	1.28	1596
11	11.5	10	14	34	1.05	1022
12	11.5	18	14	34	1.05	1022
13	11.5	14	10	27	1.2	1260
14	11.5	14	18	43	1.38	810
15	11.5	14	14	34	1.05	1022

In all cases, the diameter of the tubes is established such that the mass flow velocity of the Heat Transfer Fluid (HTF) at nominal conditions is set at 3.6 m/s, with some margin from the maximum velocity. This is a critical factor that influences the overall efficiency of the system and needs to be maximized to achieve the highest possible thermal efficiency. So the tube diameter is a variable of our design which is previously established.

It can be observed that as the receiver diameter increases, the tube diameter decreases. This is because for lower receiver diameters, the radiation flux density is higher, and the total absorbed energy along the HTF path is also higher. An increase in tube diameter results in an increase in flow, which depends on the squared diameter, and an increase in the total amount of energy, which depends linearly on the tube diameter, so an increase in tube diameter tends to keep constant the temperature increment. The same principle applies to the number of faces; as this number increases, the length of the path that the HTF follows increases, and also does the total amount of energy, necessitating an increase in tube diameter to compensate for this.

The number of tubes primarily increases with the receiver diameter because the receiver is larger, and the tube diameter is lower. This number decreases as the number of faces increases since the tube diameter

increases and the receiver area only slightly increases. Meanwhile, the height of the receiver does not affect the number of tubes.

The gaps among the tubes are adjusted to cover the entire panel length with a minimum value to avoid tube contact.

The number of circuits considered for all the designs is 2 with no crossovers and the flow path for both circuits goes from N to S. This flow path reduces film temperatures and so the defocusing of the mirrors optimizing the yearly energy produced [2]. It is planned to analyze also these parameters in future works, but it is not expected important results modifications.

4. Results discussion and optimization

The heliostat field is optimized in the initial stage of the optimization process. For this purpose, heliostats of 12·10 m were considered and the optimized tower height was 250 m for all the cases. The layout for each case is summarized in Table 4.

Table 4. Heliostat layout for each case.

Cases	D (m)	H (m)	Number of faces (-)	Number of heliostats (-)	Number of rows (-)
1	8	10	10	6451	55
2	15	10	10	5644	51
3	8	18	10	5918	52
4	15	18	10	5390	48
5	8	10	18	6451	55
6	15	10	18	5644	51
7	8	18	18	5918	52
8	15	18	18	5390	48
9	8	14	14	6003	53
10	15	14	14	5451	49
11	11.5	10	14	5780	52
12	11.5	18	14	5390	48
13	11.5	14	10	5451	49
14	11.5	14	18	5451	49
15	11.5	14	14	5451	49

This layout only varies with receiver diameter and height.

Once the heliostat field is optimized for each case, the aiming coefficient is determined, which maximizes the yearly thermal energy output. As an illustration, an optimization example for case 12 is depicted in Fig. 3. The yearly energy production is normalized with the maximum value.

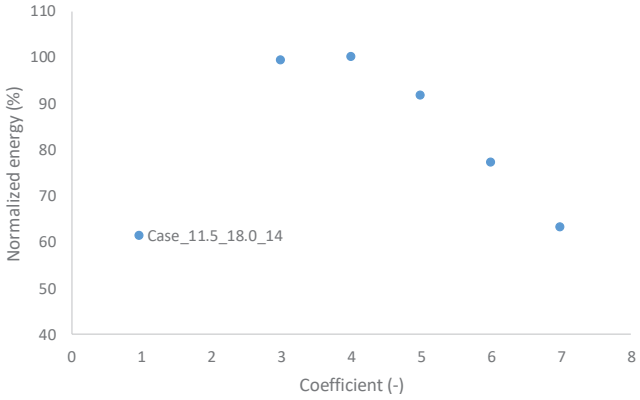

Figure 3. Normalized energy production for case 12

The results for, considering an optimum aiming strategy for each case are summarized in Table 5.

https://doi.org/10.52202/069564-0149

Table 5. Case matrix main results.

Cases	D (m)	H (m)	N. of faces (-)	Number of tubes (-)	Total energy (GWh/y)	η_{opt} (-)	η_t (-)	ΔP (bar)
1	8	10	10	670	497.60	47.28	81.33	1.14
2	15	10	10	2010	552.03	54.44	81.44	2.12
3	8	18	10	670	558.10	53.87	83.72	5.70
4	15	18	10	2000	531.56	54.19	78.11	5.47
5	8	10	18	432	513.15	47.42	84.64	23.28
6	15	10	18	1332	549.76	53.01	83.08	8.18
7	8	18	18	432	519.01	53.83	78.96	16.82
8	15	18	18	1332	542.07	53.96	80.34	15.86
9	8	14	14	532	509.10	50.56	81.06	5.53
10	15	14	14	1596	553.77	54.00	81.40	7.34
11	11.5	10	14	1022	544.25	53.82	81.42	2.53
12	11.5	18	14	1022	557.69	53.96	82.88	12.16
13	11.5	14	10	1260	562.14	54.00	82.82	4.32
14	11.5	14	18	810	563.23	53.90	83.79	24.01
15	11.5	14	14	1022	565.86	53.96	84.10	9.85

Only two cases have a greater pressure drop than the limit. This situation is considered for the optimum design.

It has been observed that the optical efficiency is optimized for each case, and the values are mostly similar, except for the cases with the lowest receiver areas. In such cases (i.e., cases 1, 5, and 9), the distribution is made more uniform to avoid exceeding the structural and corrosion limits at the radiation flux peak. As the area is small, spillage losses are high. As the receiver area increases, more rays hit the receiver with more uniform distributions, which helps avoid exceeding the structural and corrosion limits. For these cases, the thermal efficiency is high, and the slope of optical efficiency becomes lower with the growing area. However, if we continue to increase the receiver area, the radiation concentration is reduced, and thus the thermal efficiency drops, while the optical efficiency only marginally increases. Based on this analysis, it can be inferred that there exists a maximum yearly performance that is related to the receiver area (as shown in Fig. 4).

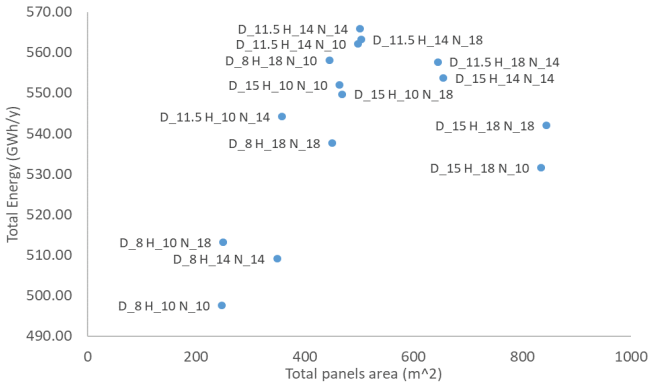

Figure 4. Yearly energy produced as a function of the receiver area.

It can be observed that the total energy produced increases with the total area of the panels up to the maximum value in the region near 500 m^2. For receiver areas greater than this value, the total energy drops. The result is not the same if the area is obtained with different combinations of values, as expected, it seems that, around the maximum value, it could exist some different combinations with similar yearly energy yield.

Once the results are obtained and analyzed, an expression that represents the yearly thermal energy as a function of the receiver diameter (D), height (H), and the number of faces (N) is obtained, Eq. (9).

$$f(D,H,N) = C_0 + C_1 \cdot D + C_2 \cdot H + C_3 \cdot N + C_4 \cdot D \cdot H + C_5 \cdot D \cdot N + C_6 \cdot H \cdot N + C_7 \cdot D^2 + C_8 \cdot H^2 + C_7 \cdot N^2 \quad (9)$$

The coefficients C_0 through C_9 are determined using the least squares method to fit the function to the data obtained from the DOE methodology. Once the coefficients are determined, this function can be potted to analyze the performance of the system as a function of the considered parameters. Figures 5(a), 5(b), and 5(c) depict the yearly energy production for cases with N = 18, N=14, and N=10, respectively. It can be noted that as the number of faces increases, the receiver height is higher and the receiver diameter is lower for the maximum value of the energy produced. So the receiver area tends to keep constant but with a different aspect ratio.

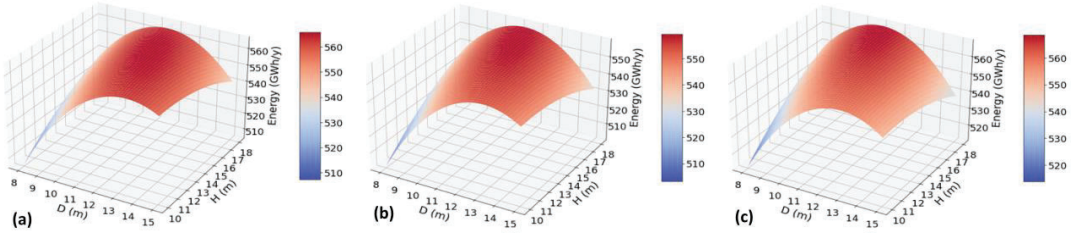

Figure 5. Total energy produced as a function of D and H for N = 18 (a), N=14 (b), and N=10 (c).

Figure 6 depicts a three-dimensional (3D) volume that displays the function value for each variable point within the considered range, represented by a color scale on the right. The volume illustrates the region where the function attains a maximum.

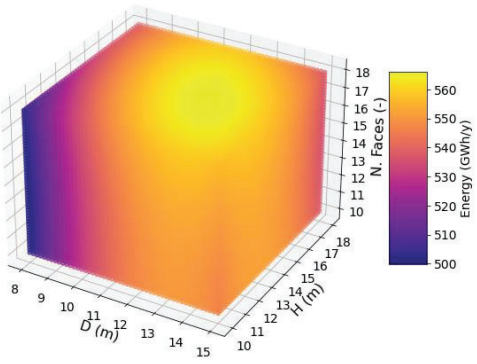

Figure 6. Total energy produced as a function of D, H, and N.

The function can be optimized to find the combination of the receiver parameters that yield the maximum yearly thermal energy. This optimization can be done using various optimization techniques, such as gradient-based methods or genetic algorithms, depending on the complexity and nonlinearity of the function. In this case, the Nelder-Mead method in Python was utilized to optimize the function within the specified range. The optimal values of the variables were determined to be (D = 12.63 m, H = 13.96 m, N = 18) which resulted in a total energy yield of 566.15 GWh/y and a receiver area of 550.3 m^2. This value is close to case 15 (D = 11.5 m, H = 14 m, N = 14), with a difference of only 0.05%. Figures 7(a) and 7(b) illustrate the areas where the response surface lies between this maximum value and yearly energy production that is 1% and 0.5% lower, respectively.

The optimal design resulting from the Nelder-Mead method would require a tube with a diameter of 40 mm and 972 tubes, which is less than the requirement for case 15. However, the receiver diameter is higher. It should be noted that the cost of the receiver is influenced by both the receiver diameter and the number of tubes required. Therefore, from a techno-economic analysis point of view, the response surface must be evaluated by taking into account the cost information to determine the optimal design. What is observed in Figures 7(a) and 7(b) is that there is an important number of combinations with similar yearly energy produced, so there is room to search for a design with a balanced cost and energy production which at the same time uses a nominal pipe size that can further reduce the costs and with a pressure drop less than 20 bar.

https://doi.org/10.52202/069564-0149

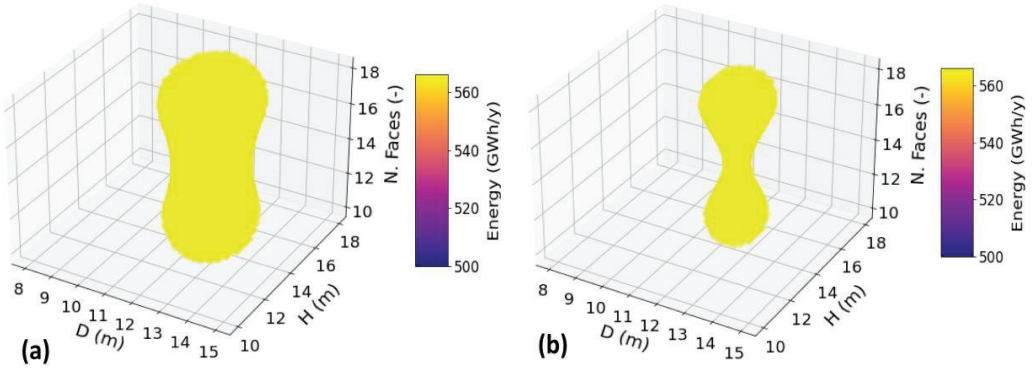

Figure 7. A volume that contains the combination of values that have yearly energy produced higher than 99% of the highest value (a) and higher than 99.5% of the highest value (b).

5. Conclusions

A methodology for the design of a CTR is proposed in this study, employing simplified models that encompass optical and thermal calculations, along with evaluations of other design constraints such as tube-failure predictions by stress or corrosion, and stable operation, which is ensured by limiting pressure drop and ensuring balanced flow among the receiver tubes. The methodology employs the yearly energy produced as the optimization criterion and considers the three primary parameters of receiver design, namely receiver diameter and height, and the number of panels. The tube diameter is predetermined for the optimization of thermal performance by controlling the HTF flow velocity.

The proposed methodology is developed in two steps, where the heliostat field is optimized for each design, followed by the optimization of the aiming strategy for the concrete heliostat field and receiver design. The employment of simplified models and DOE methodology to optimize the design enables the objective to be achieved within a reasonable time and with reduced computational resources. The response surface function obtained provides useful information for designing and optimizing solar receivers for maximum yearly thermal energy.

The results of the study indicate that for a target power of concentrated radiation flux density of 340 MWt (for one of the towers), the receiver area that optimizes the design is around 550 m^2, with an average value of 618 kWt/m^2. The results also reflect that some combinations of parameters will output similar yearly energy productions, thereby enabling the proposal of a design with similar performance and reduced costs.

Future work will include sensitivity analysis for the thermal-performance-related parameters to analyze their effect on the region for optimal designs. Furthermore, the inclusion of receiver costs as a function of the design parameters to obtain a response surface weighted by these cost estimations, oriented to reduce the Levelized Cost of Electricity (LCOE) for the optimized design will be explored. The implementation of more complex aiming strategies that can adjust heliostat aiming longitudinally in addition to vertically, to adapt the distribution to comply with the AFD without defocusing, will also be investigated.

Acknowledgments

This work has been supported by the Spanish Ministry of Economy and Competitiveness through the PID2019-110283RB-C31 project.

Nomenclature

C	response surface coefficient
coef	optimization coefeccient for the aiming strategy
f	friction factor,
d	diameter, m
E	Young Modulus, GPa
G′(z)	derivative of the characteristic function
H	receiver height, m
N	number of panels,
NTU	Number of Transfer Units
IND (t)	instantaneous beam insolation

L tube length, m

$\dot{m}$ mass flow rate, kg/s

T temperature, K

UTS Ultimate tensile strength, MPa

x^* non-dimensional coordinate,

z characteristic variable for the thermal performance equation

Greek symbols

β thermal expansion coefficient, K^{-1}

Δ difference,

γ coefficient of thermal expansion, mm/m·K

η efficiency,

ϕ radiation flux matrix for each node, kW/m^2

φ aiming point correction matrix, $kW/m^{2,}$

ν Poisson's ratio,

ρ fluid density, kg/m^3

σ thermal stress, MPa; aiming error,

Subscripts and superscripts

0 inlet

aa atmospheric attenuation

c crown

cos cosine factor

int interception

obj objective

ref reflection

$s\&b$ shading and blockages

w wall

References

[1] Pacheco JE. Results of molten salt panel and component experiments for solar central receivers: cold fill, freeze/thaw, thermal cycling and shock, and instrumentation tests. Sandia National Laboratories; 1995

[2] María de los Reyes Rodríguez Sánchez. On the design of solar external receivers. PhD thesis. Universidad Carlos III, September 2015.

[3] Abe, Osami, Utsunomiya, Taizo & Hoshino, Yoshio 1984 The thermal stability of binary alkali metal nitrates. Thermochimica Acta 78 (1-3), 251–260.

[4] Babcock & Wilcox Company, 1984. Molten Salt Receiver Subsystem Research Experiment Phase 1 – Final Report, Volume 1 – Technical. Barberton, Ohio.

[5] L.L. Vant-Hull, The role of "allowable flux density" in the design and operation of molten-salt solar central receivers, J. Sol. Energy Eng. 124 (2) (2002) 165, doi:10.1115/1.1464124, http://solarenergyengineering.asmedigitalcollection.asme.org/article.aspx?articleid¼1456457.

[6] Z. Liao, X. Li, C. Xu, C. Chang, Z. Wang. Allowable flux density on a solar central receiver, Renew. Energy 62 (2014) 747–753, doi:10.1016/j.renene.2013.08.044, http://linkinghub.elsevier.com/retrieve/pii/S0960148113004606.

[7] Alberto Sánchez-González *, María Reyes Rodríguez-Sánchez, Domingo Santana. Allowable solar flux densities for molten-salt receivers: Input to the aiming strategy. Results in Engineering 5 (2020) 100074

[8] G. Augsburger, "Thermo-economic optimisation of large solar tower power plants," Tech. Rep. (EPFL, 2013).

[9] Shuang Wang, Charles-Alexis Asselineau, John Pye, et al.An efficient method for aiming heliostats using ray-tracing. AIP Conference Proceedings 2445, 120023 (2022); https://doi.org/10.1063/5.0085672

[10] Arslan A. Rizvi, Syed N. Danish, Abdelrahman El-Leathy, Hany Al-Ansary, Dong Yang. A review and classification of layouts and optimization techniques used in design of heliostat fields in solar central receiver systems. Solar Energy 218 (2021) 296–311; https://doi.org/10.1016/j.solener.2021.02.011

https://doi.org/10.52202/069564-0149

[11] J. Serrano-Arrabal, J.J. Serrano-Aguilera, A. Sánchez-González. Dual-tower CSP plants: optical assessment and optimization with a novel cone-tracing model Renewable Energy 178 (2021) 429e442.

[12] Praveen R. P. Performance Analysis and Optimization of Central Receiver Solar Thermal Power Plants for Utility Scale Power Generation. Sustainability 2020, 12, 127; doi:10.3390/su12010127.

[13] S.M. Besarati, D. Yogi Goswami, A computationally efficient method for the design of the heliostat field for solar power tower plant, Renew. Energy 69 (2014) 226-232.

[14] C.J. Noone, M. Torrilhon, A. Mitsos, Heliostat field optimization: a new computationally efficient model and biomimetic layout, Sol. Energy 86 (2) (2012) 792-803.

[15] X. Wei, Z. Lu, Z. Wang, W. Yu, H. Zhang, Z. Yao: A new method for the design of the heliostat field layout for solar tower power plant, Renew. Energy 35 (9) (2010a) 1970-1975.

[16] X. Wei, Z. Lu, W. Yu, Z. Wang: A new code for the design and analysis of the heliostat field layout for power tower system, Sol. Energy 84 (4) (2010b) 685-690.

[17] Schwarzbözl, P., Pitz-Paal, R., Schmitz, M., Visual HFLCAL – A Software Tool for Layout and Optimization of Heliostats Fields. Presented at SolarPACES (2009), Berlin, Germany.

[18] G. Ortega, A. Rovira, A new method for the selection of candidates for shading and blocking in central receiver systems, Renew. Energy 152 (2020) 961-973.

[19] G. Ortega, A. Rovira, Proposal and analysis of different methodologies for the shading and blocking efficiency in central receivers systems, Sol. Energy 144 (2017) 475-488.

[20] G. Ortega, A. Rovira, Advanced methodologies for the calculation of shading & blocking and interception efficiency in central receiver systems, Presented at SolarPACES (2017), Santiago de Chile, Chile.

[21] Ortega, G. Transformaciones homográficas aplicadas a la simulación y optimización del subsistema óptico en centrales termosolares de torre. Ph.D. Thesis, Universidad Nacional de Educación a Distancia, Madrid, Spain, June 2017. (In Spanish)

[22] R Barbero, A. Rovira, M. J. Montes, J. M. Martínez Val, (2016). A new approach for the prediction of thermal efficiency in solar receivers. Energy Conversion and Management 2016, 123: 498–511.

[23] Rodríguez-Sánchez, M.R.; Soria-Verdugo, A.; Almendros-Ibáñez J.A; Acosta-Iborra A. & Santana, D. 2014a Thermal design guidelines of solar power towers. Applied Thermal Engineering 63 (1), 428–438.

[24] Kistler BL. A user's manual for DELSOL3: a computer code for calculating the optical performance and optimal system design for solar thermal central receiver plants. USA: Sandia National Laboratories; 1986. Sandia Report, SAND-86-8018.

[25] Robert Flesch, Cathy Frantz, Daniel Maldonado Quinto, Peter Schwarzbozl.Towards an optimal aiming for molten salt power towers. Solar Energy 155 (2017) 1273–1281; http://dx.doi.org/10.1016/j.solener.2017.07.067.

[26] Typical Meteorological Year International Weather for Energy Calculation (TMY IWEC). Available at: https://bigladdersoftware.com/epx/docs/8-3/auxiliary-programs/source-weather-data-formats.html#:~:text=The%20IWEC%20data%20files%20are,U%20S%20National%20Climatic%20Data%20Center.

[27] The ASME Boiler and Pressure Vessel Code Section III American Society of Mechanical Engineers. ASME boiler and pressure vessel code e section III, rules for construction of nuclear power plant components, Div. 1, Subsection NH; 2007. New York.